



HAL
open science

PLA-PEG forming worm-like nanoparticles despite unfavorable packing parameter: Formation mechanism, thermal stability and potential for cell internalization

Baptiste Robin, Ludivine Mousnier, Hung Lê, Nadège Grabowski, David Chapron, Ophélie Bellance-Mina, Nicolas Huang, Florence Agnely, Elias Fattal, Nicolas Tsapis

► To cite this version:

Baptiste Robin, Ludivine Mousnier, Hung Lê, Nadège Grabowski, David Chapron, et al.. PLA-PEG forming worm-like nanoparticles despite unfavorable packing parameter: Formation mechanism, thermal stability and potential for cell internalization. *International Journal of Pharmaceutics*, 2023, 643, pp.123263. 10.1016/j.ijpharm.2023.123263 . hal-04172728

HAL Id: hal-04172728

<https://hal.science/hal-04172728>

Submitted on 28 Jul 2023

HAL is a multi-disciplinary open access archive for the deposit and dissemination of scientific research documents, whether they are published or not. The documents may come from teaching and research institutions in France or abroad, or from public or private research centers.

L'archive ouverte pluridisciplinaire **HAL**, est destinée au dépôt et à la diffusion de documents scientifiques de niveau recherche, publiés ou non, émanant des établissements d'enseignement et de recherche français ou étrangers, des laboratoires publics ou privés.

PLA-PEG forming worm-like nanoparticles
despite unfavorable packing parameter:
formation mechanism, thermal stability and
potential for cell internalization

*Baptiste Robin^{1†}, Ludivine Mousnier^{1†}, Hung Lê¹, Nadège Grabowski¹, David Chapron¹,
Ophélie Bellance-Mina¹, Nicolas Huang¹, Florence Agnely¹, Elias Fattal¹, Nicolas
Tsapis^{1*}*

¹ Université Paris-Saclay, CNRS, Institut Galien Paris-Saclay, 91400, Orsay, France

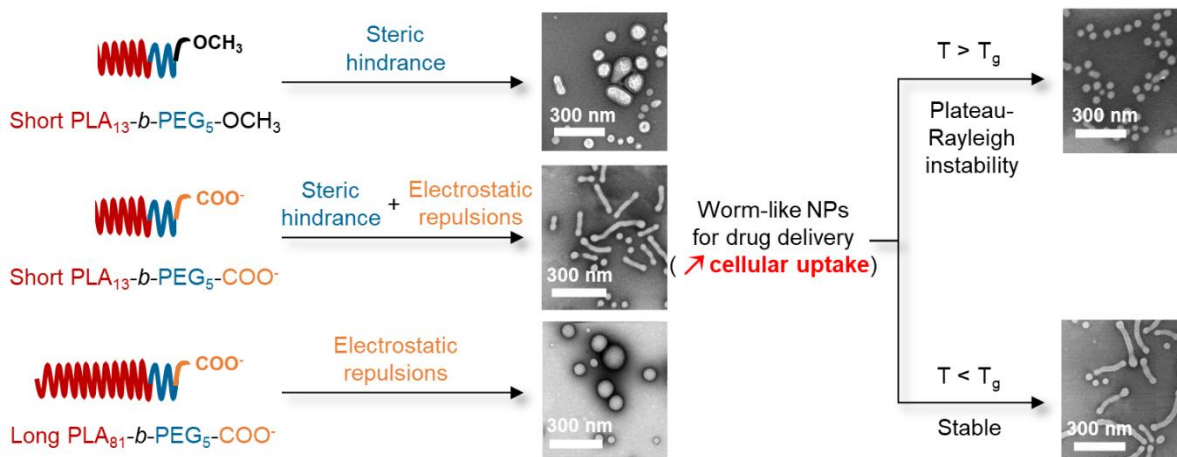
† equal contribution

KEYWORDS

Worm-like nanoparticles; anisotropic particle; PLA-PEG; emulsion-evaporation; self-assembly; glass transition temperature; cellular uptake, drug delivery.

ABSTRACT

Most nanoparticles produced for drug delivery purposes are spherical. However, the literature suggests that elongated particles are advantageous, notably in terms of cellular uptake. Thus, we synthesized biocompatible polylactide-b-poly(ethylene glycol) (PLA-PEG) polymers bearing carboxylate moieties, and used them to formulate worm-like nanoparticles by a simple emulsion-evaporation process. Worm-like nanoparticles with variable aspect ratio were obtained by simply adjusting the molar mass of the PLA block: the shorter the molar mass of the PLA block, the more elongated the particles. As PLA molar mass decreased from 80,000 g/mol to 13,000 g/mol, the proportion of worm-like nanoparticles increased from 0 to 46%, in contradiction with the usual behavior of block polymers based on their packing parameter. To explain this unusual phenomenon, we hypothesized the shape arises from a combination of steric and electrostatic repulsions between PEG chains bearing a carboxylate moiety present at the dichloromethane-water interface during the evaporation process. Worm-like particles turned out to be unstable when incubated at 37°C, above polymer glass transition temperature. Indeed, above T_g , a Plateau-Rayleigh instability occurs, leading to the division of the worm-like particles into spheres. However, this instability was slow enough to assess worm-like particles uptake by murine macrophages. A slight but significant increase of internalization was observed for worm-like particles, compared to their spherical counterparts, confirming the interest of developing biocompatible anisotropic nanoparticles for pharmaceutical applications such as drug delivery.



1. INTRODUCTION

Since the early work of Bangham on liposomes in the 60s (Bangham et al., 1965), many types of nanoparticles (NPs) of different materials have been proposed for drug delivery (Lorscheider et al., 2019; Pardeike et al., 2009; Asgari et al., 2019; Astete and Sabliov, 2006; Jamkhane et al., 2019). However, mostly spherical particles have been considered for drug delivery purposes. Indeed, the particle formation mechanism often implies interfacial tension phenomena, which favor the spherical shape, due to the minimization of surface energy.

For several years now, some studies have highlighted the possible advantages of anisotropic polymer particles in drug delivery, in particular, with elongated shapes such as rod-like (straight rigid cylinders) or worm-like particles (winding flexible cylinders) (Chen et al., 2015a; Zhou et al., 2013a). Differences between elongated and spherical particles are notably shown in terms of circulation time, targeting, and drug release (Chen et al., 2015b). First, the shape of particles impacts their *in vivo* circulation in the bloodstream due to the balance between margination forces driving particles closer to

the walls and hydrodynamic dislodging forces forcing the alignment of particles along the bloodstream (Wang et al., 2018). Particle shape governs the balance between margination and dislodging forces, inducing a reduction or an increase of the circulation time. Rigid nanorods with a length below a critical value of 500 nm exhibit a blood circulation time three-fold higher than spheres (Arnida et al., 2011; Zhou et al., 2013b). Similar behavior was observed with flexible worm-like particles (Geng et al., 2007). However, some studies also showed the higher circulation time could be due to a lower uptake by the immune system (Arnida et al., 2011). Besides this effect of particle shape on the circulation time, Safari *et al.* also demonstrated the interest of elongated particles by showing *in vitro* that the wall adhesion of rod-like particles was improved of 18-25% compared to spheres (Safari et al., 2018). In addition, the shape of particles can influence cellular uptake, beneficial when the therapeutic target is intracellular. Elongated NPs were shown to internalize faster than spheres in several cell lines (Gratton et al., 2008; Guo et al., 2018; Pada et al., 2019). Finally, the shape of particles could have an influence on drug release kinetics (Champion et al., 2007). Indeed, for a given particle volume, anisotropic particles release the drug faster than spherical ones, because of their larger surface area (Safari et al., 2018). Some authors even showed that using elongated particles slows down the release rate and prevents burst release (Fan et al., 2014), although these results remain controversial, as other teams did observe burst release with rod-like particles (Safari et al., 2018).

Given the possible advantages of non-spherical particles, many methods have emerged to produce them, such as microfluidic processes (Gregoritz et al., 2018), film stretching (Ho et al., 1993), or electrospinning (Bhaskar et al., 2010, 2009). For pharmaceutical use, nanosized vehicles are preferred as they can be safely injected

intravenously and are more efficiently internalized by cells (Gratton et al., 2008; Zheng and Yu, 2016). Electrospinning techniques do not allow to produce particles of such small size. The film stretching method, on the other hand, can be used on many types of polymer spherical nanosized particles (Ho et al., 1993). It was notably applied to biocompatible poly(lactide-co-glycolide)-b-poly(ethylene glycol)-b-poly(lactide-co-glycolide) particles, to obtain nanorods with a width of around 100 nm for a length comprised between 300 and 600 nm (Fan et al., 2014). Microfluidic was also used to produce elongated polymer NPs (Tan et al., 2020; Wang et al., 2011). However, those two techniques need specific equipment to be performed, which limits their use. A simpler method is polymerized-induced self-assembly (PISA) of block copolymers, which can generate spheres, vesicles or elongated micelles, based on the polymer packing parameter (Zhu and Nicolas, 2022; Blanazs et al., 2012; Fielding et al., 2014; LaRue et al., 2006; Zhang et al., 2011). But the method that is mostly used to prepare biocompatible elongated particles is the co-solvent evaporation process. Indeed, it has been applied on preformed biocompatible polymers, such as poly(lactide)-b-poly(ethylene glycol) (Jelonek et al., 2015) or poly(γ -benzyl-L-glutamate) (Cauchois et al., 2013), suggesting a potential use for the production of pharmaceutical anisotropic NPs.

Here, we propose an additional preparation platform of elongated polymer particles for pharmaceutical use, based on a simple emulsion-evaporation process. Close to the co-solvent evaporation method, this method has already been used to produce elongated particles with a nanometric width, by adjusting process parameters (stirring speed, surfactant concentration, pH of the continuous phase, etc) (Geng and Discher, 2005a; Heslinga et al., 2009; Safari et al., 2018). In this study, an emulsion-evaporation method

was used to prepare worm-like particles with both width and length of nanometric size, which was never done before. The NPs were made of biocompatible and partially biodegradable polylactide-b-poly(ethylene glycol) (PLA-PEG) copolymers bearing a carboxylate moiety at the PEG extremity (Casalini and Perale, 2012; Makadia and Siegel, 2011; Pandey and Jain, 2015). With no change in the process parameters, only by tuning the structure of the polymer (molar mass of the PLA block and the end-group of the PEG block), we managed to form worm-like NPs. The original mechanism underlying the formation of such particles despite unfavorable packing parameter was elucidated. Worm-like particle thermal stability was then assessed, prior to biological experiments. Morphology changes occurring at 37°C are discussed and an original hypothesis is proposed to explain them. Finally, in vitro cellular uptake of worm-like particles was evaluated on macrophages, in comparison with spherical NPs.

2. EXPERIMENTAL METHODS

2.1. Materials

D,L-Lactide was purchased from Biovalley, Polysciences Inc. (USA) and was used directly without purification. α -hydroxy- ω -carboxy-poly(ethylene glycol) (noted as HO-PEG₅₀₀₀-COOH, $M_n = 4847$ g/mol) and α -hydroxy- ω -methoxy-poly(ethylene glycol) (noted as HO-PEG₅₀₀₀-OCH₃, $M_n = 5056$ g/mol) were purchased from Iris Biotech GmbH (Germany). Stannous 2-ethyl-hexanoate (stannous octoate, 95%), deuterated chloroform, toluene (anhydrous 99.8%), and sodium cholate were provided by Sigma-Aldrich (France). Chloroform and dichloromethane were purchased from Carlo-Erba Reagents (Italy). Diethyl ether and tetrahydrofuran were provided by VWR Chemicals (USA). PLGA-rhodamine B conjugate (LA:GA ratio of 50:50, $M_w = 10,000$ – $30,000$ g/mol) was purchased from Akina Inc. (USA). Sodium dihydrogen phosphate was provided by

Rectapur (USA), while citric acid was provided by Fluka (USA). Water was purified (resistivity of 18.2 M Ω .cm) using a MilliQ Direct Type 1 Ultrapure water system (Merck Millipore, France). RAW 264.7 murine macrophages cell line was supplied by the *American Type Culture Collection* (USA). DMEM growth medium, penicillin/streptomycin mixture, and fetal bovine serum were purchased from Lonza (Switzerland).

2.2. PLA-*b*-PEG-COOH synthesis and characterization

In a two-neck round-bottom flask previously flame-dried and under a flow of inert gas, D,L-lactide, HO-PEG₅₀₀₀-COOH (or HO-PEG₅₀₀₀-OCH₃) and stannous octoate (1.5 mol PEG/mol stannous octoate) were dissolved into 10 to 12 mL of anhydrous toluene, and placed into an oil bath at 125 °C (precise amounts in Supporting Information 1). The ring opening polymerization using HO-PEG₅₀₀₀ as a macro initiator was carried out under stirring for 55 to 107 min, depending on the required final molar mass. The reaction was stopped by simply dipping the flask into cold water. After evaporation of toluene under vacuum, the polymer was dissolved into chloroform and precipitated into cold diethyl ether. Once filtered out of the diethyl ether, the polymer was dissolved into tetrahydrofuran and precipitated into water. Then, the polymer was filtered out of water, fast frozen by immersion in liquid nitrogen and left in a freezer-drier Alpha 2-4 LD (Christ, Germany) for 24h. The condenser temperature was set at -80°C and the pressure was lower than 1 mbar. After drying, the polymer was stored in sealed vials at -20°C.

The number-averaged molar mass M_n of the polymers was assessed by ¹H nuclear magnetic resonance (¹H NMR) measurements (Bruker Avance-300 MHz spectrometer, USA). Analyses were performed in 5-mm diameter tubes at a concentration of 20

mg/mL in deuterated chloroform. The molar mass M_n of PLA was calculated based on the molar mass M_n of the PEG block provided by the supplier. ^1H NMR (300 MHz, CDCl_3 , δ , ppm): 5.10-5.28 (CHCH_3COO), 3.64 (OCH_2CH_2), 1.52-1.61 (CHCH_3COO).

The dispersity of the PLA-*b*-PEG polymers was assessed by size exclusion chromatography (SEC, EcoSEC HLC-8320 GPC, from Tosoh, Japan) with two columns (PL-gel MIXED-D 300 \times 7.5 mm, beads diameter 5 μm ; linear part 4×10^2 to 4×10^5 g/mol, from Polymer Laboratories, UK). The detection was performed thanks to a differential refractometer (RI-150 SpectraSYSTEM, from Thermo Electron Corp, USA). The calibration curve was based on poly(methyl methacrylate) (PMMA) standards (Polymer Laboratories, UK). Samples were filtered on a 0.2 μm PTFE filter before being analyzed at 35°C in chloroform (HPLC grade) at a flow rate of 1 mL/min. Toluene was used as a flow rate marker.

2.3. NP preparation

PLA-*b*-PEG was dissolved into 2 mL of dichloromethane. This organic solution was then emulsified into 10 mL of 1.5% w/v sodium cholate aqueous solution using a vortex for 1 min, followed by sonication for 1 min using a sonication probe at an output power of 300W (Digital Sonifier 250, Branson). Dichloromethane was then evaporated under magnetic stirring at 300 rpm for about 3 h at 20°C. The surfactant was removed performing an ultracentrifugation cycle of 1h at 50,000 g at 4°C (LE-80K Ultracentrifuge Beckman Coulter OptimaTM). The purification method was previously optimized for sodium cholate removal, with very good results (Diou et al., 2012). The final pellet of particles was resuspended in water. For internalization studies, NPs were fluorescently labelled, by replacing 5% w/w of the total PLA-*b*-PEG-COOH with poly(lactide-co-glycolide) copolymer conjugated to rhodamine-B (PLGA-Rhodamine B,

$M_w = \sim 30,000$ g/mol, Akina Inc., USA). Labelled NPs were prepared following the same protocol as unlabeled NPs, except that the sample had to be protected from light. No difference was observed in terms of size and morphology.

2.4. NP characterization

2.4.1. Transmission Electron Microscopy (TEM)

NPs were observed in the few days following their preparation, using a JEOL 1400 electron microscope (Jeol Ltd, Japan) operating at 80 kV fitted with a SC1000 Orius camera (Gatan Inc, USA). A copper grid coated with a carbonated formvar film was plasma processed, making its surface hydrophilic. A 5- μ L drop of particle suspension (0.2 to 0.5 mg/mL depending on formulations) was deposited on the grid, and left for 30 s before blotting it with a filter paper. Then a 5- μ L drop of phosphotungstic acid solution (2% w/v) was deposited on the grid, and left for 10 s, before blotting. The phosphotungstic acid deposition was performed twice, to ensure a sufficient negative staining of the particles. NP size and shape were determined by measuring manually a hundred of particles on the TEM images, using Fiji software (Schindelin et al., 2012). NPs were mainly characterized by their diameter for spheres, their length and width for worm-like particles, and their aspect ratio (length/width ratio). For spherical particles, the aspect ratio must be close to 1. Measurements were done on at least 100 nanoparticles, found on at least two different images at different places on the grid.

2.4.2. Micro-Differential Scanning Calorimetry (Micro-DSC)

Measurements were performed using a MicroCal VP-DSC instrument (Malvern Panalytical, USA) at a scan rate of 60 K/h from 10°C to 60°C under approximately 25 psi positive cell pressure. Prior to sample analysis and after cell cleaning, six heating/cooling cycles with water in both sample and reference cells were performed.

All six heating cycles were found to be reproducible, so the suspension of PLA₁₃-*b*-PEG₅-COOH 18k NPs could be analyzed. The NP concentration of 50 mg/mL allowed to identify thermal transitions of the sample. A total of three heating/cooling cycles were recorded and the third heating scan was found to be representative. The feedback mode/gain was set on high. Thermograms were analyzed using the MicroCal Origin software (version 7) to yield the glass transition temperature at 60 K/h by the tangent method.

2.5. Evaluation of NP internalization

2.5.1. Cell culture

RAW 264.7 murine macrophages were cultured at 37 °C in a 5% CO₂ atmosphere, in DMEM growth medium, supplemented with 50 U/mL of penicillin, 50 U/mL of streptomycin, and 10% of fetal bovine serum (Lonza). Cells were divided twice a week at a ratio between 1/6 and 1/8 after detachment by scraping. After thawing, cells were used for experiments from passage 6 to 15.

2.5.2. Confocal Laser Scanning Microscopy (CLSM)

First, 30,000 cells suspended in 300 µL medium were seeded on 8-well IBIDI µ-Slides (IBIDI GmbH, Germany). After 24 h, the supernatants were discarded, replaced by NPs (PLA₈₁-*b*-PEG₅-COOH spherical NPs or PLA₁₃-*b*-PEG₅-COOH worm-like NPs) suspended in fresh medium at a concentration of 0.1 mg/mL a non-toxic concentration (Giacalone et al., 2018), and incubated at 37 °C. After 4 h and 24 h of incubation with particles, the µ-Slides were imaged with an inverted microscope (TCS SP8–gated STED, Leica Microsystems, Germany) equipped with a WLL laser and a HC PL APO CS2 63x/1.40 oil immersion objective lens. A 552-nm excitation wavelength was used, and bandwidth detection was set between 580 and 640 nm to collect the corresponding

“red” fluorescence emission of rhodamine B. To avoid reflection, a hybrid detector under gated mode (0.5-6.5 ns) was used for the fluorescence images, collected with the pinhole set at 1.0 Airy unit. A classical detector was used for the transmission images. Twelve-bit numerical images were acquired with a definition of 1024 x 1024 pixels, by mean of Leica SP8 LAS AF software (Version 3.6; Leica, Germany).

2.5.3. Flow cytometry

A sample of 500,000 cells suspended in 1 mL medium were seeded in 12-well plates. After 24 h, the supernatants were discarded, replaced by NPs (PLA₈₁-*b*-PEG₅-COOH spherical NPs or PLA₁₃-*b*-PEG₅-COOH worm-like NPs) suspended in fresh medium at a non-toxic concentration of 0.1 mg/mL (Supporting Information 2), and incubated at 37°C. After 4 h and 24 h of incubation, the supernatants were discarded, and the wells were rinsed twice with 0.5 mL of PBS. Cells were then harvested by scraping and collected in tubes. The uptake kinetic profiles of particles were assessed using a flow cytometer Accuri C6 (BD Biosciences, USA). The Mean Fluorescence Intensity (MFI) was recorded on FL-2 channel. Results are presented as the difference of the mean fluorescence intensity between samples and untreated cells, corrected by the relative fluorescence between spherical NPs and worm-like NPs. Experiments were performed 4 times in triplicate. The four average values obtained for each condition were used to perform statistical tests, to compare the internalization of PLA₈₁-*b*-PEG₅-COOH and PLA₁₃-*b*-PEG₅-COOH NPs using Prism 5 (GraphPad Software, USA), applying a nonparametric Mann-Whitney test on the data at each timepoint.

3. RESULTS

3.1. Polymer characterization

Four PLA-*b*-PEG copolymers of different molar mass and end-groups were obtained by ring-opening polymerization of lactide using OH-PEG as macroinitiators. Their denomination and characteristics are gathered in **Table 1**. We observed molar masses of 18,000, 52,000 and 86,000 g/mol: the difference between these values (only due to the PLA block molar mass) is significant, as PLA₁₃-*b*-PEG₅-COOH has a degree of polymerization of PLA (DP_{PLA}) four-fold lower than PLA₄₇-*b*-PEG₅-COOH, and six-fold lower than PLA₈₁-*b*-PEG₅-COOH. The dispersity (Đ) of the polymers was low, with values comprised between 1.15 and 1.2. Other publications describing the impact of the molar mass of diblock polymers on the shape of particles use polymers in the same range of degree of polymerization (Jelonek et al., 2015), so different particle shapes were expected with these three polymers. Also, we obtained two polymers with equivalent molar masses (18,000 g/mol) but different end-groups, COOH or OCH₃.

Table 1. Characteristics of the synthesized copolymers.

Sample ID	Copolymer denomination	Copolymer characteristics			
		M _n (g/mol) by ¹ H NMR	DP _{PLA} by ¹ H NMR	M _n (PLA)/M _n (total) by SEC	Đ by SEC
1	PLA ₁₃ - <i>b</i> -PEG ₅ -COOH	17,900	181	0.73	1.15
2	PLA ₄₇ - <i>b</i> -PEG ₅ -COOH	51,500	648	0.90	1.18
3	PLA ₈₁ - <i>b</i> -PEG ₅ -COOH	85,600	1122	0.94	1.20
4	PLA ₁₃ - <i>b</i> -PEG ₅ -OCH ₃	18,500	187	0.72	1.25

3.2. Parameters influencing NP shape

The three acid-ending polymers with different molar masses were used to prepare NPs by emulsion-evaporation. NPs were observed by TEM (**Figure 1a-c**) and characterized by their size and average aspect ratio (**Table 2**). First, the sample corresponding to PLA₁₃-*b*-PEG₅-COOH contained worm-like NPs and spheres in comparable proportions, 46 and 54%, respectively. The average ratio of these NPs was 1.61. PLA₄₇-*b*-PEG₅-COOH also produced a blend of spheres and worm-like NPs, but mostly composed of spheres (93%), leading to an average aspect ratio of 1.18. Finally, PLA₈₁-*b*-PEG₅-COOH only led to spheres, with an aspect ratio close to 1. Thus, the shorter the PLA block, the more numerous the worm-like NPs. This phenomenon could also be followed by DLS, with a higher pdl for PLA₁₃-*b*-PEG₅-COOH (0.208 ± 0.020) than for PLA₈₁-*b*-PEG₅-COOH (0.127 ± 0.016), attesting the increased worm-like NP population (Supporting Information 4). However, DLS was not further used for size characterization, as it is meaningless when particles are not spherical (Larsen, 2017).

In addition, the average diameter of the spheres was similar to the width of the worm-like NPs (between 40 and 50 nm), suggesting that spheres could derive from worm-like NPs (or the other way around). PLA₁₃-*b*-PEG₅-COOH was the only polymer providing a narrow distribution of sphere diameters (49 ± 7 nm). For PLA₄₇-*b*-PEG₅-COOH and PLA₈₁-*b*-PEG₅-COOH, the average diameter was close to 50 nm also, but the distribution was wide, with standard deviations around 20 nm.

Another interesting feature of worm-like NPs was their undulations and bulb-shaped extremities, similar to a Plateau-Rayleigh instability (**Figure 1a-crop**). Jain *et al.* suggest that some polymer molar mass and dispersity ranges could favor the sensitivity of the

NPs to these undulations, but the mechanism driving the formation of these undulations remains unexplained (Jain and Bates, 2004).

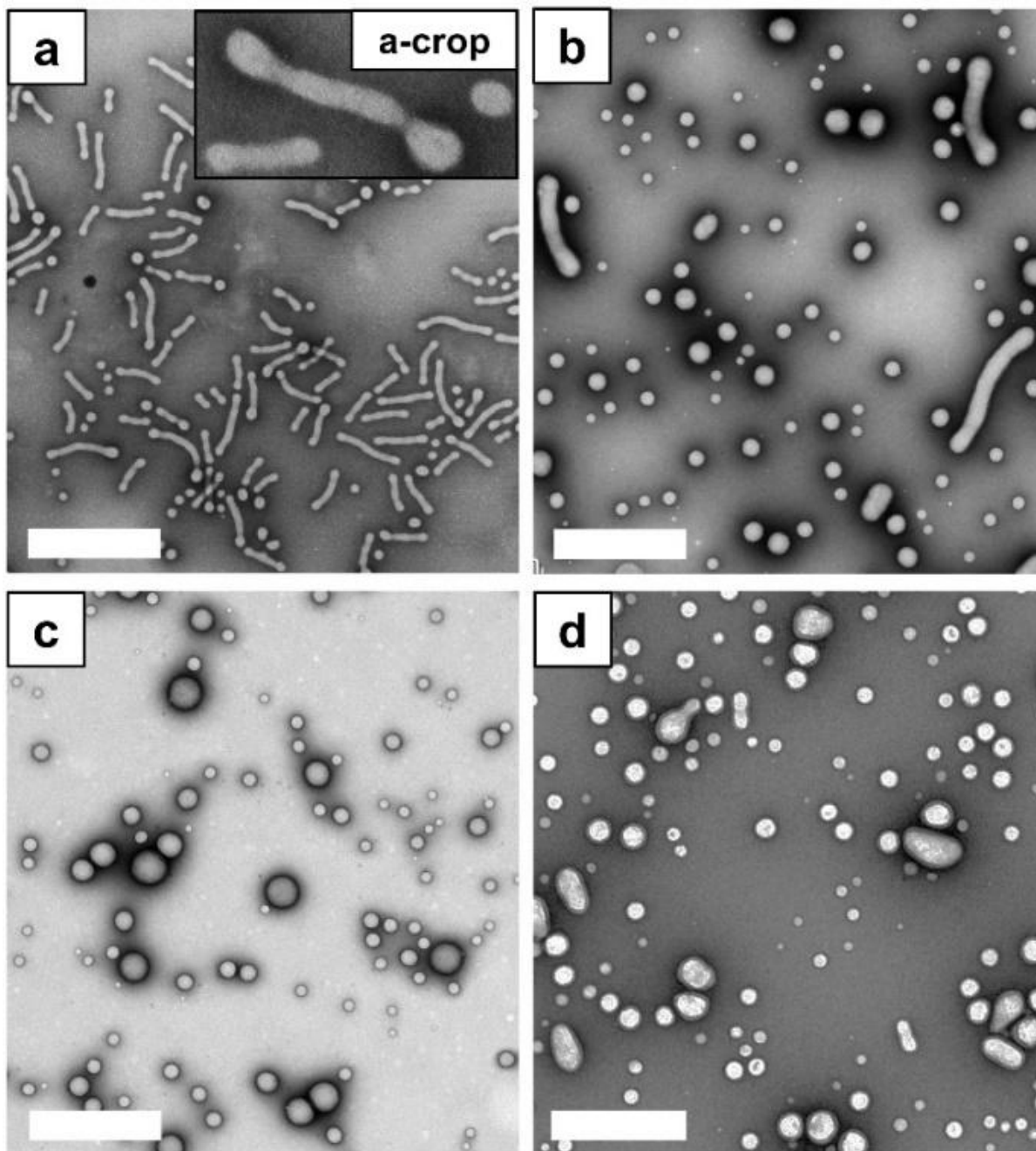


Figure 1: TEM images of NPs obtained with acid-ending copolymers of different molar mass: (a) $\text{PLA}_{13}\text{-}b\text{-PEG}_5\text{-COOH}$, (b) $\text{PLA}_{47}\text{-}b\text{-PEG}_5\text{-COOH}$, (c) $\text{PLA}_{81}\text{-}b\text{-PEG}_5\text{-COOH}$ and (d) $\text{PLA}_{13}\text{-}b\text{-PEG}_5\text{-OCH}_3$ (Scale bar: 500 nm). A cropped image of (a) shows the undulations of a worm-like NP. Additional zoomed out images are provided in Supporting Information 3.

Table 2. Morphological characteristics (TEM) and ζ -potential (DLS, in 1 mM NaCl) of the NPs obtained with the different copolymers. NA: Not Applicable. NM: not measured.

Samples	Spherical NPs	Worm-like NPs		Average aspect ratio		% worm-like NPs	ζ -potential (mV)
	Diameter (nm)	Width (nm)	Length (nm)	All NPs	Worm-like NPs only		
PLA ₁₃ - <i>b</i> -PEG ₅ -COOH NPs	49 ± 7	38 ± 5	157 ± 69	1.61	4.1	46	-23.3 ± 3.0
PLA ₄₇ - <i>b</i> -PEG ₅ -COOH NPs	55 ± 18	59 ± 9	201 ± 107	1.18	3.4	7	NM
PLA ₈₁ - <i>b</i> -PEG ₅ -COOH NPs	51 ± 21	NA	NA	1.10	NA	0	-35.8 ± 2.5
PLA ₁₃ - <i>b</i> -PEG ₅ -OCH ₃ NPs	59 ± 14	66 ± 20	140 ± 36	1.20	2.1	10	-15.5 ± 1.3

Not only the molar mass of the PLA block has a dramatic effect on the particle shape, but the PEG block end-group is also an important parameter. Indeed, replacing the COOH end-group of the PEG block by OCH₃ on PLA₁₃-*b*-PEG₅ allowed the formation of very short unregular rods, instead of the long worm-like NPs observed with COOH end-group (**Figure 1d**). This might be due to a difference of charge between the two copolymers: the COOH end groups undergo a deprotonation at pH = 7.2, leading to negatively charged carboxylates whereas OCH₃ end groups remain neutral. This hypothesis is supported by the zeta potential values: OCH₃ ending polymer gave a lower zeta potential to the NPs (- 15 mV) compared to the COOH ending polymer of similar molar mass (- 23 mV).

3.3. Thermal stability of worm-like NPs

The thermal stability of worm-like NPs obtained with PLA₁₃-*b*-PEG₅-COOH was assessed by incubating suspensions at either 4, 20, 37 and 60°C. The average aspect ratio was calculated overtime for each temperature (**Figure 2**). First, we observed a

very good stability of the particle shape at 4 and 20°C, as the average aspect ratio remained around 1.8. At 37°C, however, we observed a fast and irreversible decrease of the average aspect ratio, reaching the value of 1.1 after 24 h. Indeed, the TEM pictures show a very large majority of spherical NPs, with only few short worm-like NPs remaining. Due to their bulb-shaped extremities, the worm-like NPs seem to have divided into spheres from their ends. The diameter of these newly formed spheres was similar to the width of the worm-like NPs, exactly like the spherical NPs initially present in the suspension. Finally, NPs incubated at 60°C also showed a very fast division into spheres, maybe even faster than the ones at 37°C as no remaining worm-like NPs were observed on TEM images. However, no aspect ratio could be measured after 3 days on the suspension at 60°C, because of an aggregation of all NPs, associated with a fast degradation of the copolymer, which molar mass decreased from 18,000 to 13,000 g/mol after 24 h (Supporting Information 5).

Even if high temperatures seem to trigger a division of the elongated NPs, we must emphasize that this phenomenon only occurred when the centrifugation step leading to sodium cholate removal was performed before heating the sample (Supporting Information 6). In other words, the division of worm-like NPs into spheres is impossible at high concentrations of sodium cholate.

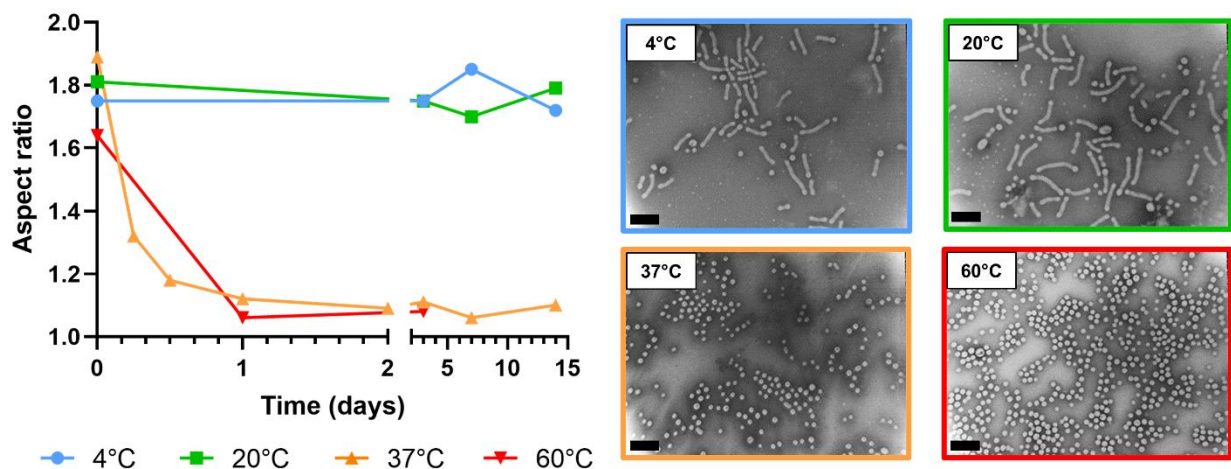


Figure 2: Evolution of the average aspect ratio of the PLA₁₃-*b*-PEG₅-COOH worm-like NPs overtime, at 4°C (blue), 20°C (green), 37°C (orange) and 60°C (red), determined on TEM images. Examples of these images are given, after storing the suspension 3 days, at the corresponding temperatures (Scale bar: 200 nm).

Finally, we performed micro-DSC on PLA₁₃-*b*-PEG₅-COOH NPs suspended either in sodium cholate 1.5% or water. The typical thermogram of a glass transition (T_g) was observed at $34.5 \pm 1^\circ\text{C}$ in both media (Supporting Information 7).

3.4. Cellular uptake of worm-like NPs

After producing and characterizing worm-like NPs, the influence of NP shape on the cellular uptake was assessed. Rhodamine-labelled worm-like PLA₁₃-*b*-PEG₅-COOH NPs and spherical PLA₈₁-*b*-PEG₅-COOH NPs were first prepared, and no change was observed compared to unlabelled NPs. They were incubated with murine macrophages for 24 h, before measuring the fluorescence of the cells (**Figure 3**). First, CLSM images clearly showed an uptake of NPs by macrophages, mostly in the cytoplasm, with an increase of the fluorescence overtime (**Figure 3a**). This trend was confirmed by flow cytometry, with an average MFI of 364 ± 44 and 514 ± 51 respectively for spherical

PLA₈₁-*b*-PEG₅-COOH NPs and worm-like PLA₁₃-*b*-PEG₅-COOH NPs after 4 h, and an average MFI of 732 ± 122 and 1092 ± 280 after 24 h (**Figure 3b**). The internalization of worm-like PLA₁₃-*b*-PEG₅-COOH was significantly higher than spherical PLA₈₁-*b*-PEG₅-COOH NPs after 4 h (p-value = 0.029), but not significant after 24 h (p-value = 0.057). This absence of significance after 24 h could be due to a wider distribution of the values.

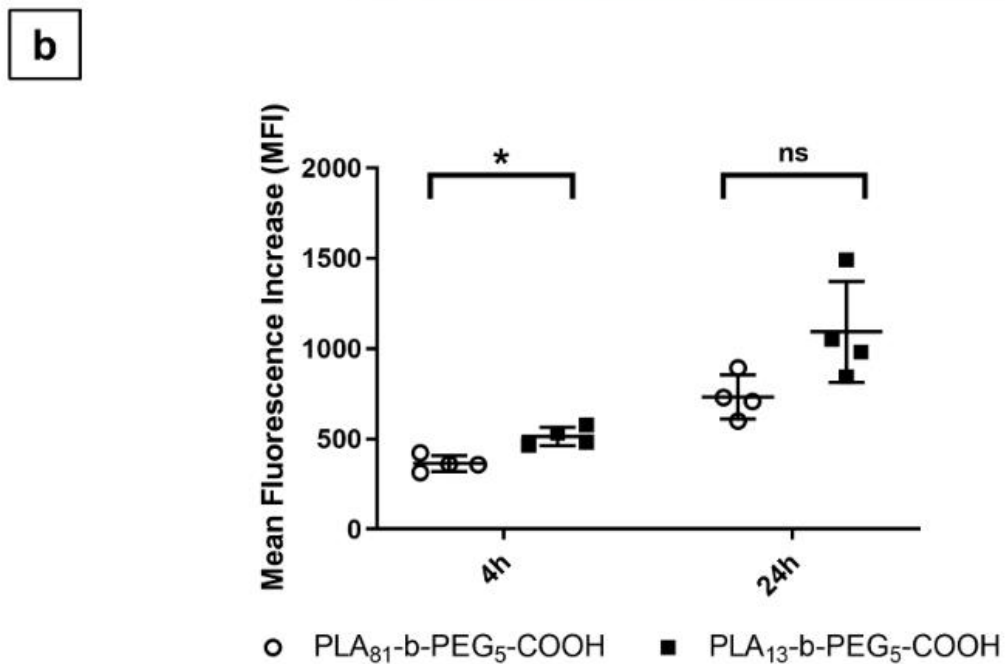
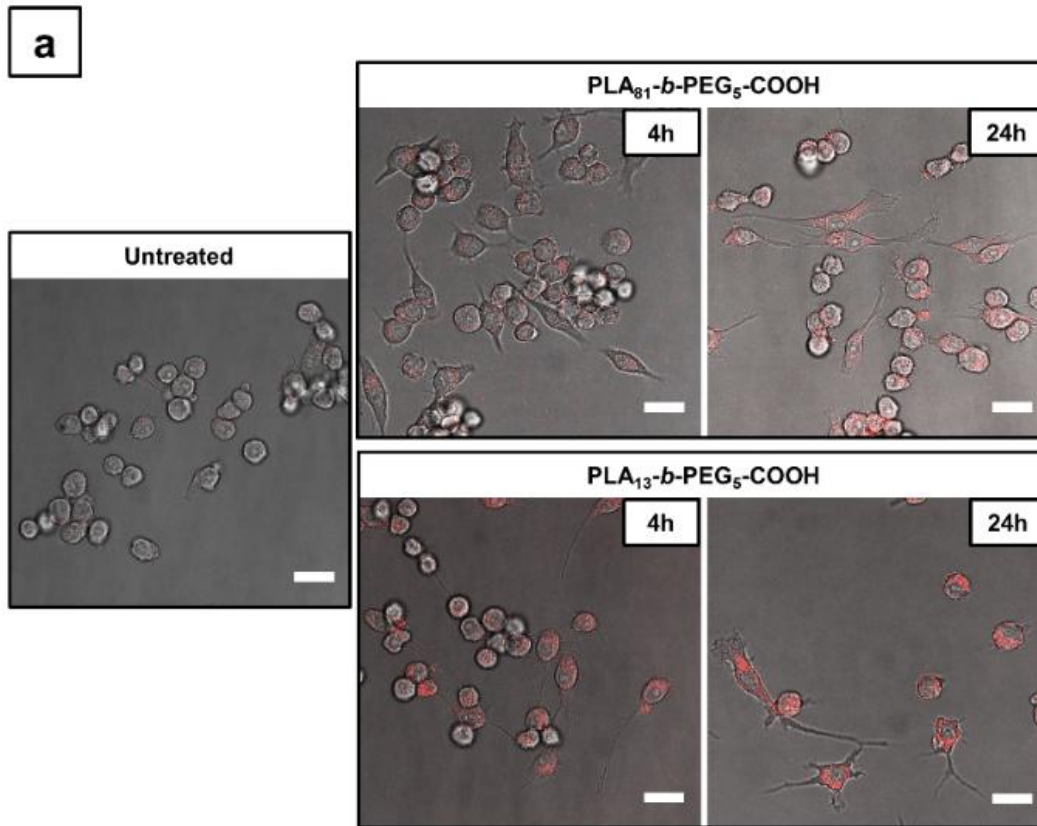


Figure 3: Internalization of rhodamine-B-labelled PLA₁₃-*b*-PEG₅-COOH worm-like NPs and PLA₈₁-*b*-PEG₅-COOH spherical NPs by RAW 264.7 cells, after 4 and 24 h, assessed by: (a)

CLSM images (Scale bar: 20 μm), and (b) Flow cytometry (*: p-value < 0.05; ns: p-value > 0.05).

4. DISCUSSION

4.1. Formation and division of worm-like NPs

The data resulting from these experiments allowed us to propose a mechanism to explain the formation of worm-like NPs. The one-dimensional aggregation of monomer-swollen spheres proposed by Armes *et al.* was first considered (Blanazs *et al.*, 2011; Fielding *et al.*, 2013). In these studies, the NPs are formed by PISA: the copolymers were prepared by aqueous dispersion polymerization, and self-assembled in structures of different shapes throughout the polymerization process, based on their packing parameter. When the hydrophobic block of the core of the particles was short, the copolymers self-assembled into spheres. The continuation of the polymerization led to a molecular frustration of the inner block in its spherical organization, leading to the aggregation and fusion of spherical NPs, forming worm-like NPs. The authors underlined that the width of the worm-like particles was similar to the diameter of the spheres to support this hypothesis (Fielding *et al.*, 2013). While the polymerization went on, another reorganization finally occurred to form vesicles. Despite the accuracy of this hypothesis to explain the shape of NPs in the case of PISA, it did not seem to fit with our results. Indeed, we did observe a similarity between the sphere diameter and the worm width, but several points differ from Armes experiments. First, the fusion of Armes' spherical NPs resulted from the increase of the copolymer molar mass, while polymerization was still on going. In our case, the worm-like NPs could not be the result

of the merging of spheres due to the continuation of polymerization, because a preformed copolymer was used. A second difference with Armes system is that PLA₁₃-*b*-PEG₅-COOH did not organize following its packing parameter. Usually, a hydrophobic block with a high volume leads to cylindrical or vesicular organizations, as it cannot pack densely into a sphere (Israelachvili, 2011). In our case, the trend of NP shape with molar masses was reversed: short hydrophobic PLA blocks form worm-like NPs, while spheres were obtained with longer PLA blocks.

Hayward *et al.* also obtained mixtures of spheres and worm-like NPs with an emulsion-evaporation process, very similar to the one we describe hereby (Zhu et al., 2009; Zhu and Hayward, 2008). However, the trend was, again, opposite to the one we observe: worm-like NPs were formed in the presence of long hydrophobic PLA blocks. This could be easily explained by the packing parameter of polymers, which does not fit with our specific situation.

Thus, another mechanism should be proposed to explain this unusual formation of worm-like NPs by emulsion-evaporation process (**Figure 4a-f**). First, both blocks of PLA₁₃-*b*-PEG₅-COOH were fully dissolved in dichloromethane droplets (**Figure 4a**). Indeed, dichloromethane is often used to prepare PLA particles (C. Mallard J. Coudane, I. Rault, 2000), and it is also known to be a better solvent for PEG than water (Tomaszewski et al., 1999). Then dichloromethane was evaporated slowly, increasing the concentration of copolymer in the droplets until reaching its solubility limit. At this point, the PEG block was probably expelled from the dichloromethane droplets to be exposed to water, as it is energetically more favorable than mixing PEG with PLA in the final solid particles (**Figure 4b**) (Pisani et al., 2009). After further evaporation of dichloromethane, the concentration of amphiphilic molecules at the interface increased

until triggering an interfacial instability, well described by Hayward *et al.* (Zhu and Hayward, 2008). This would have promoted the formation of a nanosized emulsion, consisting of dichloromethane-swelled PLA₁₃-*b*-PEG₅-COOH assemblies dispersed in water (**Figure 4c**). The PEG chains exposed to the aqueous medium probably generated steric hindrance at the surface, more pronounced for PLA₁₃-*b*-PEG₅-COOH as the relative PEG content is higher in this copolymer (Zhang *et al.*, 2009). Also, in the case of PLA₁₃-*b*-PEG₅-COOH, the number of chains is about 4.5 times higher than with PLA₈₁-*b*-PEG₅-COOH, for a given weight concentration. Therefore, to accommodate all the PEG chains PLA₁₃-*b*-PEG₅-COOH requires more surface than PLA₈₁-*b*-PEG₅-COOH. However, this surface increase occurred at constant volume, so the spherical droplets underwent an elongation, leading to cylinders (Daoud and Williams, 1995) (**Figure 4d**). If this hypothesis can lead to shapes that contradict the predictions based on the packing parameter, it is supported by the observation that NP elongation was further favored by the electrostatic repulsions arising from the carboxylate end-group of PEG, while the methoxy end-group led to less elongated NPs (**Figure 1** and **Table 2**).

Also, the elongated droplets were not perfectly cylindrical but displayed undulations similar to a Plateau-Rayleigh instability (Jain and Bates, 2004). Shortly, any tiny perturbation in a long liquid cylinder can spread and grow, leading to a sinusoidal undulation of the cylinder surface. If the wavelength of this undulation is higher than π times the diameter, then the modulated cylinder is more stable than a regular cylinder and the system reaches an equilibrium. But if the undulation wavelength is lower than this critical value, the modulated cylinder is unstable, and breaks out into small spherical droplets following Laplace-Young equation (Eggers, 1997; Rayleigh, 1878). Thus, we assume that the cylindrical dichloromethane-swelled PLA₁₃-*b*-PEG₅-COOH assemblies

underwent this Plateau-Rayleigh instability, leading to the formation of undulations and a division into spheres. This explains the presence of spheres with a diameter equal to the width of the worm-like NPs. Finally, as the dichloromethane finished evaporating, the elongated particles froze before the end of their complete division, leading to a blend of spheres and worm-like NPs (**Figure 4e**). If our experimental conditions did not allow to obtain samples with 100% of worm-like NPs, although it might be needed for some applications. Some modifications of the process were experimented, such as evaporating dichloromethane under vacuum to “freeze” the worm-like NPs before they divide by Plateau-Rayleigh instability. However, this adaptation of the protocol did not improve the worm-like NP fraction at the end of the evaporation (data not shown). Separation methods were also tested, for example ultracentrifugation or ultrafiltration. But worm-like NP width and spherical diameter are equal, making their separation difficult (if not impossible) by these techniques (data not shown). Cross-flow filtration and preparative electrophoresis were also considered, but they required big amounts of NP suspensions and specific equipment we could not access.

In addition, we observed that this division into spheres could be triggered again, even after the complete evaporation of dichloromethane, by increasing the temperature to 37°C (**Figure 2**). Similar temperature-dependent shape modifications were already described in the literature. Geng *et al.* showed the division of worm-like NPs made of poly(ethylene oxide)-*b*-(ϵ -caprolactone) into spherical NPs at 37°C. However, the mechanism was different, because it involved a reorganization of the copolymer following its degradation (Geng and Discher, 2005b), whereas we showed there was no PLA hydrolysis during particle division (Supporting Information 5). Armes' team also observed a division of poly(lauryl methacrylate)-poly(benzyl methacrylate) worm-like

NPs by heating them up. This phenomenon was described as reversible. The mechanism proposed was based on a better solvation of the core at high temperatures, leading to a modification of the curvature. This mechanism did not suit to our system, because we did not observe any reversibility (Fielding et al., 2014). In fact, the division of worm-like NP into spheres might be a consequence of the low glass transition temperature T_g of PLA₁₃-*b*-PEG₅-COOH polymer (34.5°C). Indeed, heating above the polymer T_g might favor the mobility of the polymer chains, making the peristaltic movements characterizing Plateau-Rayleigh instability possible again, re-starting the division of cylindrical particles into spheres. This spontaneous phenomenon has already been observed on solid polystyrene strips, undergoing Plateau-Rayleigh instability until their division into spheres just by annealing them above their T_g (Park et al., 2006). Nevertheless, the rubbery NPs might be more difficult to break than dichloromethane-containing droplets, so a high interfacial tension between the NPs and the medium was necessary. This would explain the non-division of worm-like NPs in presence of a high concentration of sodium cholate, that reduced the interfacial tension too low to trigger the separation of spheres from the cylinder extremities. Thus, heating the worm-like NPs above 34.5°C in purified water led to their total and irreversible division (**Figure 4f**).

It must be noted this division mechanism should lead to a homogeneous population of spheres, with a diameter comparable to the cylinder length. If this is the case for PLA₁₃-*b*-PEG₅-COOH (before and after heating at 37°C), we observed a wider distribution of sphere diameters with PLA₄₇-*b*-PEG₅-COOH and PLA₈₁-*b*-PEG₅-COOH. This could mean that only a part of the spheres resulted from the division of elongated droplets, containing the shortest polymers of the distribution. The bigger spheres might have formed in one step, with the longest polymers chains.

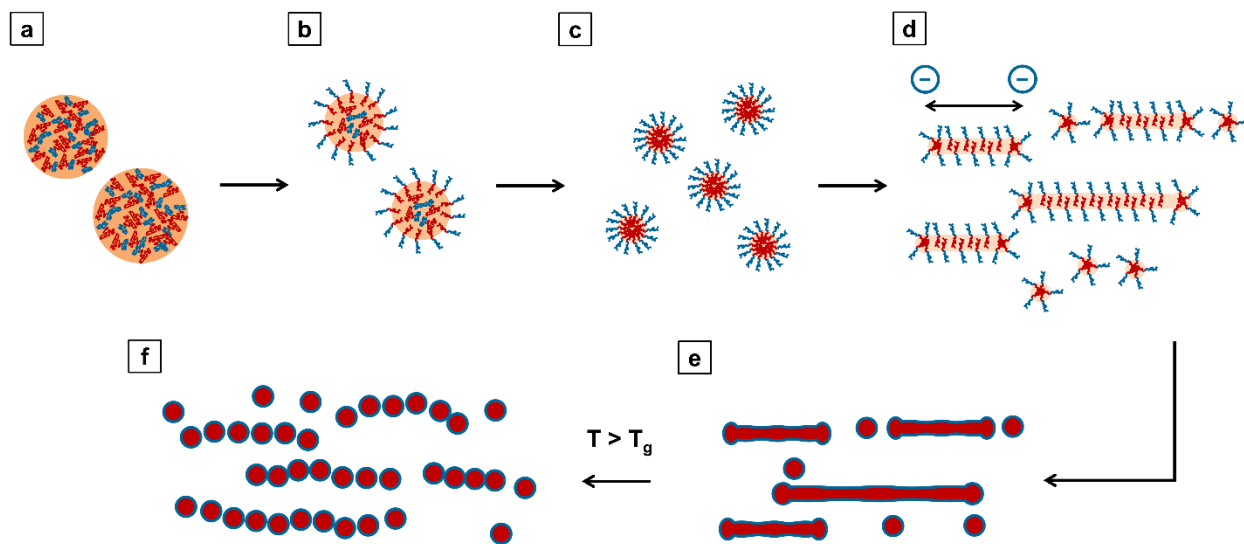


Figure 4: Scheme illustrating the formation and evolution of the worm-like NPs morphology composed of PLA₁₃-*b*-PEG₅-COOH. (a) The two blocks of the copolymer were dissolved in dichloromethane droplets dispersed in the aqueous phase. (b) The progressive evaporation of dichloromethane increased the PEG concentration inside the droplets, forcing the expulsion of this latter towards water. (c) Further evaporation of dichloromethane increases the concentration of amphiphilic molecules at the interface, until triggering an interfacial instability, and the formation of a nanosized emulsion. (d) The presence of all the charged PEG blocks at the interface probably induced steric hindrance and electrostatic repulsions, hence the surface increase and droplet elongation. This elongation caused Plateau-Rayleigh instability, leading to the apparition of undulations and a division of the cylindrical droplets from their extremities into smaller spherical droplets. (e) The total evaporation of dichloromethane froze the system, hence the existence of both worm-like and spherical NPs. (f) The heat could reactivate the Plateau-Rayleigh instability if the temperature exceeded the T_g of the polymer, progressively leading to the complete division of the worm-like NPs. Scheme not to scale.

4.2. Cellular uptake of worm-like NPs

The cellular uptake of spherical PLA₈₁-*b*-PEG₅-COOH NPs and worm-like PLA₁₃-*b*-PEG₅-COOH NPs showed a significant difference after 4 h of incubation, as described earlier. This result, obtained with RAW 264.7 murine macrophages, might appear in contradiction with the literature. Indeed, Mitragotri group (Champion and Mitragotri, 2006; Sharma et al., 2010) and others after them (Safari et al., 2020) showed macrophages internalize elongated particles less efficiently than spheres, because the phagocytosis of those particles requires a great actin-remodeling, which is an energy-consuming process. However, most of these publications are dealing with particles that have at least one dimension in the micrometer-range. Yet it is known that, depending on the particle size, internalization mechanisms can be very different. Indeed, while submicron particles undergo phagocytosis, NPs which size is lower than 500 nm would actually be internalized by other endocytosis processes such as clathrin-mediated endocytosis, which only requires a local modest rearrangement of the cytoskeleton (Decuzzi et al., 2008). Other publications also mention macropinocytosis and caveolae-mediated endocytosis as potential mechanisms involved in NP internalization (Bannunah et al., 2014). Thus, it is important to compare the cell uptake we observe with results obtained with other nanometric vehicles.

For this particle size range (< 500 nm), literature seems to confirm our results. Indeed, several publications showed that elongated NPs of various materials undergo a higher cell uptake, by many cell types such as HeLa (Gratton et al., 2008), 4T1 (Guo et al., 2018) or Caco-2 (Zheng et al., 2017) cancer cells, or even NIH/3T3 fibroblasts (Xue et al., 2018). Gratton *et al.* explained the better internalization of elongated NPs by the higher area of contact surface of cylinders, which increases the interactions with cell membranes (Gratton et al., 2008). However, those publications might not be the most

relevant ones to discuss our results, as it compares the uptake of elongated and spherical NPs with similar volume or hydrodynamic diameter, which is not our case. The worm-like NPs presented here have a width equivalent to the spherical NP diameter. They are more comparable to the work of Chithrani *et al.* who studied the uptake of gold NPs of different size and shapes, including spheres with a diameter equivalent to the nanorod width (Chithrani *et al.*, 2006). Surprisingly, this article is one of the few concluding on a lower uptake of elongated NPs. It compared nanorods of 14 x 74 nm with spherical NPs of 14 nm, and showed that HeLa cells took up 3.75-fold more spheres than nanorods, which, at first sight, is at odds with our results. But the authors measured the number of NPs internalized, while we measured the mean fluorescence intensity, which gives an information about the volume of NP internalized. Thus, if we calculate the volume of the gold particles used by Chithrani *et al.* they are approximately of 11,000 nm³ for the nanorods versus 1,500 nm³ for the spheres, so a nanorod has a volume 7.3-fold higher than a sphere. Thus, if HeLa cells took up 3.75-fold more spheres than nanorods, uptaken nanorods represent a volume that is 2-fold higher than the uptaken spheres, which follows the same trend than our results.

If these articles are in good agreement with the results exposed here, none of them used macrophages for the uptake study. Thus we can compare our result with Arnida *et al.*, who used RAW 264.7 murine macrophages to compare the cell uptake of gold spheres of 50 nm and nanorods of 10 x 45 nm (Arnida *et al.*, 2011). This publication showed a lower internalization of nanorods by macrophages, which might seem to invalidate our results. Yet, the authors moderated the significance of their results, as cell uptake of the spheres could have been favored by both their surface charge and geometry. Indeed, in absence of serum, nanorods are almost neutral (+1 mV) while

spheres are negative (-27 mV), which allows interactions with scavenger receptors and uptake (Arnida et al., 2011; Safari et al., 2020; Tabata and Ikada, 1988). Even if the ζ -potential of the spheres is lowered in presence of serum, the difference of uptake might remain significant and influence the uptake (Yu et al., 2012). In our case, the improved internalization by macrophages after 4 h was not due to the ζ -potential of the NPs, as worm-like PLA₁₃-*b*-PEG₅-COOH NPs are less negative than spherical PLA₈₁-*b*-PEG₅-COOH NPs (respectively -23.3 mV versus -35.8 mV in 1 mM NaCl, Table 2). The results of Arnida *et al.* can also be discussed through the particle size that were used. Indeed, the spherical NPs had a diameter similar to the nanorod length, which gives a developed surface area 5-fold higher and a volume 18-fold higher than the nanorods. This is clearly in favor of the sphere uptake (Yu et al., 2012), which can explain the difference between the conclusion of Arnida's study and the present one.

Thus, this comparison with literature data allows us to hypothesize the uptake increase in the first four hours was due to the worm-like shape of PLA₁₃-*b*-PEG₅-COOH NPs, even if nothing is clear and discussion remains open. Indeed, it is difficult to compare studies as they rarely use the same cell lines, which may change the internalization pathways. Also, authors compare spheres and elongated NPs with similar hydrodynamic radius, or similar volume, or similar surface, length, width, etc. This is not an issue to analyze the result of a single study, but it makes it very difficult to compare several studies. Thus, as long as authors do not agree on the size parameter to be fixed to compare spheres and anisotropic particles, drawing general conclusions about the influence of particle shape will remain complicated.

Between 4 and 24 h of incubation, the internalization kinetics seemed to change. The cell uptake of PLA₁₃-*b*-PEG₅-COOH NPs was no more significantly different to the cell

uptake of spherical PLA₈₁-*b*-PEG₅-COOH NPs after 24 h of incubation. In fact, this phenomenon cannot be discussed apart from the thermal stability of worm-like NPs. Indeed, worm-like NPs divide into spheres when temperature exceeds the T_g of PLA₁₃-*b*-PEG₅-COOH. Given that the incubation of NPs with cells was performed at 37°C during 24 h, in absence of sodium cholate, we assume worm-like PLA₁₃-*b*-PEG₅-COOH NPs underwent a division into spheres as described earlier. Thus, the results of the internalization study must be discussed cautiously. First, the significant difference of cell MFI between the PLA₈₁-*b*-PEG₅-COOH NPs and the PLA₁₃-*b*-PEG₅-COOH NPs after 4 h of incubation could be due to the presence of worm-like NPs. Indeed, if both samples contained spherical NPs of similar diameter (around 50 nm), some worm-like PLA₁₃-*b*-PEG₅-COOH NPs remained undivided after 4 h of incubation, as the average aspect ratio was still around 1.6 (**Figure 2**). Therefore, the worm-like shape could have slightly increased the uptake by murine macrophages. Then, if this trend seemed to be confirmed after 24 h of incubation (the average MFI was still higher with PLA₁₃-*b*-PEG₅-COOH NPs), the difference between the two samples was not significant anymore. Indeed, the proportion of worm-like NPs decreasing very fast at 37°C, both samples contained only spheres after 24 h (**Figure 2**). The uptake rate of the two samples, although different at early times, probably tended to converge, hence the MFI difference was not significant anymore. As we observed a slight increase of the cell MFI only during the first four hours, we can hypothesize that a higher volume of PLA₁₃-*b*-PEG₅-COOH NPs was internalized only while worm-like NPs were present in the sample.

5. CONCLUSION

We have shown the ability of PLA-*b*-PEG-COOH to form worm-like NPs by an emulsion-evaporation process, under specific conditions. First, a short PLA block

(13,000 g/mol) increased the content of PEG at the interface, inducing steric hindrance. This led to an increase of the particle surface to accommodate all the PEG chains, hence the elongation of the NPs into worm-like NPs during the solvent evaporation. Also, the deprotonation of the carboxyl end group of the PEG block ensured electrostatic repulsions, further increasing the length of the worm-like NPs. However, as any fluid cylinder, the worm-like NPs underwent a Plateau-Rayleigh instability, generating undulations at their surface and leading to their division into spherical droplets, from the worm extremities. After all the solvent has evaporated, the structures were frozen, explaining the mixture of spherical and worm-like NPs observed. This instability could however be recovered by increasing the temperature above the copolymer T_g , after purifying the NP suspension from surfactants. This led to a complete division of the worm-like NPs into spheres after 24 h at 37°C. Finally, preliminary results showed the interest of worm-like NPs for drug delivery purposes, as they might be significantly more taken-up by murine macrophage cells in the first four hours of incubation.

To conclude, this new method allows to produce biocompatible anisotropic NPs for drug delivery. These NPs were produced with a simple technique and showed first encouraging results in terms of cellular uptake. However, more studies are necessary to reach higher rates of worm-like NPs, and to make worm-like NPs more stable at physiological temperature. It would allow us to better assess their actual benefit for intracellular drug-delivery. Whether this mechanism of formation of the worm-like particles can be extended to other polymers should also be evaluated.

6. ASSOCIATED CONTENT

6.1. Supporting Information in a single file

Detailed synthesis conditions, Cell viability, DLS analysis of the NPs (size and ζ -potential), TEM images at lower magnification, Degradation of the PLA block during the division of worm-like NPs, Effect of the presence of cholate sodium on the division of the worm-like NPs, Determination of the glass transition temperature of PLA13-b-PEG5-COOH worm-like NPs suspended in water.

7. AUTHOR INFORMATION

Corresponding Author

Nicolas Tsapis
Institut Galien Paris-Saclay, UMR CNRS 8612,
Faculté de Pharmacie, Université Paris-Saclay
17 Avenue des sciences, 91400 Orsay, FRANCE
Phone 33 1 80006091
nicolas.tsapis@universite-paris-saclay.fr

8. ACKNOWLEDGMENTS

N. Huang acknowledges the Agence Nationale de la Recherche (ANR) for its support through a Young Researchers grant (ANR-16-CE09-0003), that funded the PhD of Baptiste Robin and the internship of Ophélie Bellance-Mina. Ludivine Mousnier's salary was supported by Laboratory of Excellence LERMIT, through a grant from ANR (ANR-10-LABX-33). Authors acknowledge financial support from ANR (Investissements d'Avenir, Nanobiotechnologies, nUCA project ANR-10-NANO-06). The present work has also benefited from Imagerie-Gif core facilities (<http://www.i2bc.paris-saclay.fr>), member of IBISA (<http://www.ibisa.net>), supported by **Agence Nationale de la Recherche** (ANR-11-EQPX-0029/Morphoscope, ANR-10-INBS-

04/FranceBioImaging ; ANR-11-IDEX-0003-02/ Saclay Plant Sciences), with the precious help of Cynthia Gillet and Claire Boulogne. Finally, we acknowledge Valérie Nicolas (Microscopy facility (MIPSIT), UAR3679 (IPSIT), Université Paris-Saclay) for her help on the LCSM experiments, Laurence Moine for fruitful discussions and Théo Pesenti for his help with SEC.

9. ABBREVIATIONS

PEG: Poly(ethylene glycol)

PLA: Polylactide

PLA-PEG: poly(lactide)-*b*-poly(ethylene glycol)

T_g: Glass transition temperature

10. REFERENCES

- Arnida, Janát-Amsbury, M.M., Ray, A., Peterson, C.M., Ghandehari, H., 2011. Geometry and surface characteristics of gold nanoparticles influence their biodistribution and uptake by macrophages. *Eur. J. Pharm. Biopharm., Biological Barriers* 77, 417–423. <https://doi.org/10.1016/j.ejpb.2010.11.010>
- Asgari, S., Saberi, A.H., McClements, D.J., Lin, M., 2019. Microemulsions as nanoreactors for synthesis of biopolymer nanoparticles. *Trends Food Sci. Technol.* 86, 118–130. <https://doi.org/10.1016/j.tifs.2019.02.008>
- Astete, C.E., Sabliov, C.M., 2006. Synthesis and characterization of PLGA nanoparticles. *J. Biomater. Sci. Polym. Ed.* 17, 247–289. <https://doi.org/10.1163/156856206775997322>
- Bangham, A.D., Standish, M.M., Watkins, J.C., 1965. Diffusion of univalent ions across the lamellae of swollen phospholipids. *J. Mol. Biol.* 13, 238-IN27. [https://doi.org/10.1016/S0022-2836\(65\)80093-6](https://doi.org/10.1016/S0022-2836(65)80093-6)
- Bannunah, A.M., Vilasaliu, D., Lord, J., Stolnik, S., 2014. Mechanisms of Nanoparticle Internalization and Transport Across an Intestinal Epithelial Cell Model: Effect of Size and Surface Charge. *Mol. Pharm.* 11, 4363–4373. <https://doi.org/10.1021/mp500439c>
- Bhaskar, S., Hitt, J., Chang, S.-W.L., Lahann, J., 2009. Multicompartmental Microcylinders. *Angew. Chem. Int. Ed.* 48, 4589–4593. <https://doi.org/10.1002/anie.200806241>
- Bhaskar, S., Pollock, K.M., Yoshida, M., Lahann, J., 2010. Towards Designer Microparticles: Simultaneous Control of Anisotropy, Shape, and Size. *Small* 6, 404–411. <https://doi.org/10.1002/sml.200901306>

- Blanazs, A., Madsen, J., Battaglia, G., Ryan, A.J., Armes, S.P., 2011. Mechanistic Insights for Block Copolymer Morphologies: How Do Worms Form Vesicles? *J. Am. Chem. Soc.* 133, 16581–16587. <https://doi.org/10.1021/ja206301a>
- Blanazs, A., Verber, R., Mykhaylyk, O.O., Ryan, A.J., Heath, J.Z., Douglas, C.W.I., Armes, S.P., 2012. Sterilizable Gels from Thermoresponsive Block Copolymer Worms. *J. Am. Chem. Soc.* 134, 9741–9748. <https://doi.org/10.1021/ja3024059>
- C. Mallard J. Coudane, I. Rault, M.V., 2000. In vitro delivery of a sparingly water soluble compound from PLA50 microparticles. *J. Microencapsul.* 17, 13–28. <https://doi.org/10.1080/026520400288526>
- Casalini, T., Perale, G., 2012. 1 - Types of bioresorbable polymers for medical applications, in: Jenkins, M., Stamboulis, A. (Eds.), *Durability and Reliability of Medical Polymers*, Woodhead Publishing Series in Biomaterials. Woodhead Publishing, pp. 3–29.
- Cauchois, O., Segura-Sanchez, F., Ponchel, G., 2013. Molecular weight controls the elongation of oblate-shaped degradable poly(γ -benzyl-L-glutamate)nanoparticles. *Int. J. Pharm.* 452, 292–299. <https://doi.org/10.1016/j.ijpharm.2013.04.074>
- Champion, J.A., Katare, Y.K., Mitragotri, S., 2007. Particle shape: A new design parameter for micro- and nanoscale drug delivery carriers. *J. Controlled Release*, Fourth International Nanomedicine and Drug Delivery Symposium 121, 3–9. <https://doi.org/10.1016/j.jconrel.2007.03.022>
- Champion, J.A., Mitragotri, S., 2006. Role of target geometry in phagocytosis. *Proc. Natl. Acad. Sci.* 103, 4930–4934. <https://doi.org/10.1073/pnas.0600997103>
- Chen, J., Clay, N.E., No-hyung Park, Kong, H., 2015a. Non-spherical particles for targeted drug delivery. *Chem. Eng. Sci., Pharmaceutical Particles and Processing* 125, 20–24. <https://doi.org/10.1016/j.ces.2014.10.022>
- Chen, J., Clay, N.E., Park, N., Kong, H., 2015b. Non-spherical particles for targeted drug delivery. *Chem. Eng. Sci., Pharmaceutical Particles and Processing* 125, 20–24. <https://doi.org/10.1016/j.ces.2014.10.022>
- Chithrani, B.D., Ghazani, A.A., Chan, W.C.W., 2006. Determining the Size and Shape Dependence of Gold Nanoparticle Uptake into Mammalian Cells. *Nano Lett.* 6, 662–668. <https://doi.org/10.1021/nl052396o>
- Daoud, M., Williams, C., 1995. *La juste argile*. Les Ed. de physique, Les Ulis.
- Decuzzi, P., Pasqualini, R., Arap, W., Ferrari, M., 2008. Intravascular Delivery of Particulate Systems: Does Geometry Really Matter? *Pharm. Res.* 26, 235. <https://doi.org/10.1007/s11095-008-9697-x>
- Diou, O., Tsapis, N., Giraudeau, C., Valette, J., Gueutin, C., Bourasset, F., Zanna, S., Vauthier, C., Fattal, E., 2012. Long-circulating perfluorooctyl bromide nanocapsules for tumor imaging by ¹⁹FMRI. *Biomaterials* 33, 5593–5602. <https://doi.org/10.1016/j.biomaterials.2012.04.037>
- Eggers, J., 1997. Nonlinear dynamics and breakup of free-surface flows. *Rev. Mod. Phys.* 69, 865–930. <https://doi.org/10.1103/RevModPhys.69.865>
- Fan, J.-B., Song, Y., Li, H., Jia, J.-P., Guo, X., Jiang, L., 2014. Controllable drug release and effective intracellular accumulation highlighted by anisotropic biodegradable PLGE nanoparticles. *J Mater Chem B* 2, 3911–3914. <https://doi.org/10.1039/C3TB21726D>
- Fielding, L.A., Derry, M.J., Ladmiral, V., Rosselgong, J., Rodrigues, A.M., Ratcliffe, L.P.D., Sugihara, S., Armes, S.P., 2013. RAFT dispersion polymerization in non-

- polar solvents: facile production of block copolymer spheres, worms and vesicles in n-alkanes. *Chem. Sci.* 4, 2081. <https://doi.org/10.1039/c3sc50305d>
- Fielding, L.A., Lane, J.A., Derry, M.J., Mykhaylyk, O.O., Armes, S.P., 2014. Thermo-responsive Diblock Copolymer Worm Gels in Non-polar Solvents. *J. Am. Chem. Soc.* 136, 5790–5798. <https://doi.org/10.1021/ja501756h>
- Geng, Y., Dalhaimer, P., Cai, S., Tsai, R., Tewari, M., Minko, T., Discher, D.E., 2007. Shape effects of filaments versus spherical particles in flow and drug delivery. *Nat. Nanotechnol.* 2, 249–255. <https://doi.org/10.1038/nnano.2007.70>
- Geng, Y., Discher, D.E., 2005a. Hydrolytic Degradation of Poly(ethylene oxide)-block-Polycaprolactone Worm Micelles. *J. Am. Chem. Soc.* 127, 12780–12781. <https://doi.org/10.1021/ja053902e>
- Geng, Y., Discher, D.E., 2005b. Hydrolytic Degradation of Poly(ethylene oxide)-block-Polycaprolactone Worm Micelles. *J. Am. Chem. Soc.* 127, 12780–12781. <https://doi.org/10.1021/ja053902e>
- Giacalone, G., Tsapis, N., Mousnier, L., Chacun, H., Fattal, E., 2018. PLA-PEG nanoparticles improve the anti-inflammatory effect of rosiglitazone on macrophages by enhancing drug uptake compared to free rosiglitazone. *Materials* 11. <https://doi.org/10.3390/ma11101845>
- Gratton, Ropp, P.A., Pohlhaus, P.D., Luft, J.C., Madden, V.J., Napier, M.E., DeSimone, J.M., 2008. The effect of particle design on cellular internalization pathways. *Proc. Natl. Acad. Sci.* 105, 11613–11618. <https://doi.org/10.1073/pnas.0801763105>
- Gregoritzka, M., Abstiens, K., Graf, M., Goepferich, A.M., 2018. Fabrication of antibody-loaded microgels using microfluidics and thiol-ene photoclick chemistry. *Eur. J. Pharm. Biopharm.* 127, 194–203. <https://doi.org/10.1016/j.ejpb.2018.02.024>
- Guo, Y., Wang, T., Zhao, S., Han, M., Dong, Z., Wang, X., Wang, Y., 2018. Amphiphilic Hybrid Dendritic-Linear Molecules as Nanocarriers for Shape-Dependent Antitumor Drug Delivery. *Mol. Pharm.* 15, 2665–2673. <https://doi.org/10.1021/acs.molpharmaceut.8b00190>
- Heslinga, M.J., Mastria, E.M., Eniola-Adefeso, O., 2009. Fabrication of biodegradable spheroidal microparticles for drug delivery applications. *J. Controlled Release* 138, 235–242. <https://doi.org/10.1016/j.jconrel.2009.05.020>
- Ho, C.C., Keller, A., Odell, J.A., Ottewill, R.H., 1993. Preparation of monodisperse ellipsoidal polystyrene particles. *Colloid Polym. Sci.* 271, 469–479. <https://doi.org/10.1007/BF00657391>
- Israelachvili, J.N., 2011. Intermolecular and surface forces, Third edit. ed. Elsevier, Academic Press, Amsterdam.
- Jain, S., Bates, F.S., 2004. Consequences of Nonergodicity in Aqueous Binary PEO–PB Micellar Dispersions. *Macromolecules* 37, 1511–1523. <https://doi.org/10.1021/ma035467j>
- Jamkhande, P.G., Ghule, N.W., Bamer, A.H., Kalaskar, M.G., 2019. Metal nanoparticles synthesis: An overview on methods of preparation, advantages and disadvantages, and applications. *J. Drug Deliv. Sci. Technol.* 53, 101174. <https://doi.org/10.1016/j.jddst.2019.101174>
- Jelonek, K., Li, S., Wu, X., Kasperczyk, J., Marcinkowski, A., 2015. Self-assembled filomicelles prepared from polylactide/poly(ethylene glycol) block copolymers for

- anticancer drug delivery. *Int. J. Pharm.* 485, 357–364. <https://doi.org/10.1016/j.ijpharm.2015.03.032>
- Larsen, G.K., 2017. Characterization of Anisotropic and Shape-Selective Nanomaterials: Methods and Challenges, in: Hunyadi Murph, S.E., Larsen, G.K., Coopersmith, K.J. (Eds.), *Anisotropic and Shape-Selective Nanomaterials: Structure-Property Relationships*, Nanostructure Science and Technology. Springer International Publishing, Cham, pp. 79–101. https://doi.org/10.1007/978-3-319-59662-4_4
- LaRue, I., Adam, M., Pitsikalis, M., Hadjichristidis, N., Rubinstein, M., Sheiko, S.S., 2006. Reversible Morphological Transitions of Polystyrene-*b*-polyisoprene Micelles. *Macromolecules* 39, 309–314. <https://doi.org/10.1021/ma051548z>
- Lorscheider, M., Tsapis, N., Ur-Rehman, M., Gaudin, F., Stolfa, I., Abreu, S., Mura, S., Chaminade, P., Espeli, M., Fattal, E., Mujeeb-ur-Rehman, Gaudin, F., Stolfa, I., Abreu, S., Mura, S., Chaminade, P., Espeli, M., Fattal, E., 2019. Dexamethasone palmitate nanoparticles: An efficient treatment for rheumatoid arthritis. *J. Controlled Release* 296, 179–189. <https://doi.org/10.1016/J.JCONREL.2019.01.015>
- Makadia, H.K., Siegel, S.J., 2011. Poly Lactic-co-Glycolic Acid (PLGA) as Biodegradable Controlled Drug Delivery Carrier. *Polymers* 3, 1377–1397. <https://doi.org/10.3390/polym3031377>
- Pada, A.-K., Desai, D., Sun, K., Prakirth Govardhanam, N., Törnquist, K., Zhang, J., Rosenholm, J.M., 2019. Comparison of Polydopamine-Coated Mesoporous Silica Nanorods and Spheres for the Delivery of Hydrophilic and Hydrophobic Anticancer Drugs. *Int. J. Mol. Sci.* 20, 3408. <https://doi.org/10.3390/ijms20143408>
- Pandey, A., Jain, D.S., 2015. Poly Lactic-Co-Glycolic Acid (PLGA) Copolymer and Its Pharmaceutical Application, in: Thakur, V.K., Thakur, M.K. (Eds.), *Handbook of Polymers for Pharmaceutical Technologies*. John Wiley & Sons, Inc., Hoboken, NJ, USA, pp. 151–172.
- Pardeike, J., Hommoss, A., Müller, R.H., 2009. Lipid nanoparticles (SLN, NLC) in cosmetic and pharmaceutical dermal products. *Int. J. Pharm.* 366, 170–184. <https://doi.org/10.1016/j.ijpharm.2008.10.003>
- Park, J., Suh, K.Y., Seo, S., Lee, H.H., 2006. Anisotropic rupture of polymer strips driven by Rayleigh instability. *J. Chem. Phys.* 124, 214710. <https://doi.org/10.1063/1.2206580>
- Pisani, E., Ringard, C., Nicolas, V., Raphaël, E., Rosilio, V., Moine, L., Fattal, E., Tsapis, N., 2009. Tuning microcapsules surface morphology using blends of homo- and copolymers of PLGA and PLGA-PEG. *Soft Matter* 5, 3054. <https://doi.org/10.1039/b902042j>
- Rayleigh, Lord, 1878. On The Instability Of Jets. *Proc. Lond. Math. Soc.* s1-10, 4–13. <https://doi.org/10.1112/plms/s1-10.1.4>
- Safari, H., Adili, R., Holinstat, M., Eniola-Adefeso, O., 2018. Modified two-step emulsion solvent evaporation technique for fabricating biodegradable rod-shaped particles in the submicron size range. *J. Colloid Interface Sci.* 518, 174–183. <https://doi.org/10.1016/j.jcis.2018.02.030>
- Safari, H., Kelley, W.J., Saito, E., Kaczorowski, N., Carethers, L., Shea, L.D., Eniola-Adefeso, O., 2020. Neutrophils preferentially phagocytose elongated particles—

- An opportunity for selective targeting in acute inflammatory diseases. *Sci. Adv.* 6, eaba1474. <https://doi.org/10.1126/sciadv.aba1474>
- Schindelin, J., Arganda-Carreras, I., Frise, E., Kaynig, V., Longair, M., Pietzsch, T., Preibisch, S., Rueden, C., Saalfeld, S., Schmid, B., Tinevez, J.-Y., White, D.J., Hartenstein, V., Eliceiri, K., Tomancak, P., Cardona, A., 2012. Fiji: an open-source platform for biological-image analysis. *Nat. Methods* 9, 676–682. <https://doi.org/10.1038/nmeth.2019>
- Sharma, G., Valenta, D.T., Altman, Y., Harvey, S., Xie, H., Mitragotri, S., Smith, J.W., 2010. Polymer particle shape independently influences binding and internalization by macrophages. *J. Controlled Release* 147, 408–412. <https://doi.org/10.1016/j.jconrel.2010.07.116>
- Tabata, Y., Ikada, Y., 1988. Effect of the size and surface charge of polymer microspheres on their phagocytosis by macrophage. *Biomaterials* 9, 356–362. [https://doi.org/10.1016/0142-9612\(88\)90033-6](https://doi.org/10.1016/0142-9612(88)90033-6)
- Tan, Z., Hou, Z., Wang, K., Li, Y., Zhang, L., Zhu, J., Xu, J., 2020. Kinetic Control of Length and Morphology of Segmented Polymeric Nanofibers in Microfluidic Chips. *Langmuir* 36, 13364–13370. <https://doi.org/10.1021/acs.langmuir.0c02904>
- Tomaszewski, K., Szymanski, A., Lukaszewski, Z., 1999. Separation of poly(ethylene glycols) into fractions by sequential liquid–liquid extraction. *Talanta* 50, 299–306. [https://doi.org/10.1016/S0039-9140\(99\)00024-7](https://doi.org/10.1016/S0039-9140(99)00024-7)
- Wang, C.-W., Sinton, D., Moffitt, M.G., 2011. Flow-Directed Block Copolymer Micelle Morphologies via Microfluidic Self-Assembly. *J. Am. Chem. Soc.* 133, 18853–18864. <https://doi.org/10.1021/ja2067252>
- Wang, Z., Wu, Z., Liu, J., Zhang, W., 2018. Particle morphology: an important factor affecting drug delivery by nanocarriers into solid tumors. *Expert Opin. Drug Deliv.* 15, 379–395. <https://doi.org/10.1080/17425247.2018.1420051>
- Xue, J., Guan, Z., Zhu, X., Lin, J., Cai, C., Jin, X., Li, Y., Ye, Z., Zhang, W., Jiang, X., 2018. Cellular internalization of polypeptide-based nanoparticles: effects of size, shape and surface morphology. *Biomater. Sci.* 6, 3251–3261. <https://doi.org/10.1039/C8BM01163J>
- Yu, S.S., Lau, C.M., Thomas, S.N., Jerome, W.G., Maron, D.J., Dickerson, J.H., Hubbell, J.A., Giorgio, T.D., 2012. Size- and charge-dependent non-specific uptake of PEGylated nanoparticles by macrophages. *Int. J. Nanomedicine* 7, 799–813. <https://doi.org/10.2147/IJN.S28531>
- Zhang, H., Bei, J., Wang, S., 2009. Multi-morphological biodegradable PLGE nanoparticles and their drug release behavior. *Biomaterials* 30, 100–107. <https://doi.org/10.1016/j.biomaterials.2008.09.016>
- Zhang, X., Boissé, S., Zhang, W., Beaunier, P., D’Agosto, F., Rieger, J., Charleux, B., 2011. Well-Defined Amphiphilic Block Copolymers and Nano-objects Formed in Situ via RAFT-Mediated Aqueous Emulsion Polymerization. *Macromolecules* 44, 4149–4158. <https://doi.org/10.1021/ma2005926>
- Zheng, M., Yu, J., 2016. The effect of particle shape and size on cellular uptake. *Drug Deliv. Transl. Res.* 6, 67–72. <https://doi.org/10.1007/s13346-015-0270-y>
- Zheng, N., Li, J., Xu, C., Xu, Lishi, Li, S., Xu, Lu, 2017. Mesoporous silica nanorods for improved oral drug absorption. *Artif. Cells Nanomedicine Biotechnol.*
- Zhou, Z., Ma, X., Jin, E., Tang, J., Sui, M., Shen, Y., Van Kirk, E.A., Murdoch, W.J., Radosz, M., 2013a. Linear-dendritic drug conjugates forming long-circulating

- nanorods for cancer-drug delivery. *Biomaterials* 34, 5722–5735. <https://doi.org/10.1016/j.biomaterials.2013.04.012>
- Zhou, Z., Ma, X., Jin, E., Tang, J., Sui, M., Shen, Y., Van Kirk, E.A., Murdoch, W.J., Radosz, M., 2013b. Linear-dendritic drug conjugates forming long-circulating nanorods for cancer-drug delivery. *Biomaterials* 34, 5722–5735. <https://doi.org/10.1016/j.biomaterials.2013.04.012>
- Zhu, C., Nicolas, J., 2022. (Bio)degradable and Biocompatible Nano-Objects from Polymerization-Induced and Crystallization-Driven Self-Assembly. *Biomacromolecules* 23, 3043–3080. <https://doi.org/10.1021/acs.biomac.2c00230>
- Zhu, J., Ferrer, N., Hayward, R.C., 2009. Tuning the assembly of amphiphilic block copolymers through instabilities of solvent/water interfaces in the presence of aqueous surfactants. *Soft Matter* 5, 2471–2478. <https://doi.org/10.1039/B818065B>
- Zhu, J., Hayward, R.C., 2008. Spontaneous Generation of Amphiphilic Block Copolymer Micelles with Multiple Morphologies through Interfacial Instabilities. *J. Am. Chem. Soc.* 130, 7496–7502. <https://doi.org/10.1021/ja801268e>